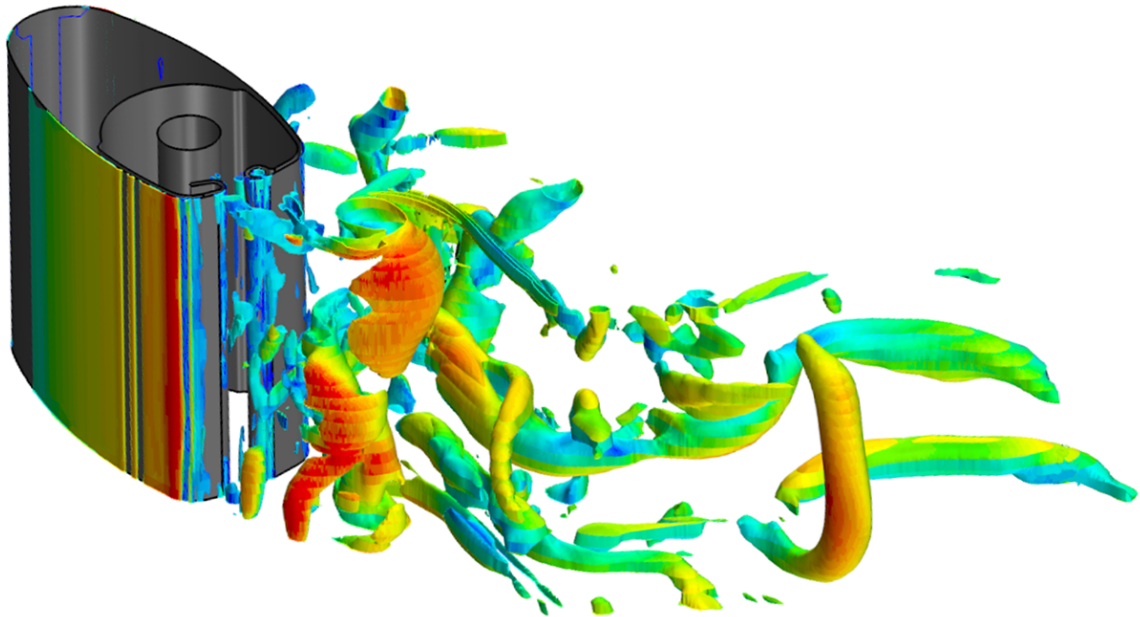




CHALMERS
UNIVERSITY OF TECHNOLOGY



Investigation of Wind-Induced Noise to Optimize Masts

Project in Applied Mechanics

JONATHAN FAHLBECK
JOHAN FORSGREN
SANKAR RAJU NARAYANASAMY
MARTIN OTTOSSON
DAVID WINQVIST

Department of Applied Mechanics
CHALMERS UNIVERSITY OF TECHNOLOGY
Gothenburg, Sweden 2017

PROJECT IN APPLIED MECHANICS 2017

Investigation of Wind-Induced Noise to Optimize Masts

JONATHAN FAHLBECK

JOHAN FORSGREN

SANKAR RAJU NARAYANASAMY

MARTIN OTTOSSON

DAVID WINQVIST



CHALMERS
UNIVERSITY OF TECHNOLOGY

Department of Applied Mechanics
Division of Fluid Mechanics
CHALMERS UNIVERSITY OF TECHNOLOGY
Gothenburg, Sweden 2017

Investigation of Wind-Induced Noise to Optimize Masts

JONATHAN FAHLBECK, JOHAN FORSGREN, SANKAR RAJU NARAYANASAMY, MARTIN OTTOSSON, DAVID WINQVIST

© JONATHAN FAHLBECK, JOHAN FORSGREN, SANKAR RAJU NARAYANASAMY, MARTIN OTTOSSON, DAVID WINQVIST, 2017.

Supervisors: Dr. Hua-Dong Yao and Prof. Lars Davidsson, Applied Mechanics, Chalmers

Examiners: Dr. Håkan Johansson and Dr. Valery Chernoray, Applied Mechanics, Chalmers

Project in Applied Mechanics 2017
Department of Applied Mechanics
Division of Fluid Mechanics
Chalmers University of Technology
SE-412 96 Gothenburg
Telephone +46 31 772 1000

Cover: An isosurface of the λ_2 criterion with the velocity magnitude visualised along the surface, for mast geometry (*b*).

Gothenburg, Sweden 2017

Abstract

In modern society the awareness of disturbing noise has increased. Thus it is of importance to find the cause of noise generation and prevent the designs which produces them. In this report the wind-induced whistling noise from two sailboat mast profiles have been evaluated. It has previously been observed that one of the profiles generates a whistling noise while the other one does not. The predetermined conditions were a free stream velocity of 20 m/s and a yaw angle of 33° . The commercial software STAR-CCM+ has been used along with aero-acoustic features. The simulations showed that no whistling noise could be identified. Although several interesting features regarding the flow around the mast geometries have been discovered, no root cause of the whistling noise could be completely established. In order to fully understand the noise generation, additional work needs to be performed on the subject. Thus it is recommended to examine more yaw angles and velocities of the incoming flow. In this manner it is the authors believe that it would be possible to finally find the answer of what is causing the whistling noise.

Keywords: Whistling, Noise, STAR-CCM+, Mast, FW-H, Aero-Acoustics, Vortex Shedding

Acknowledgements

First of all we would like to thank our supervisor Hua-Dong Yao. Without his continuous support and advice, the overall understanding and progress within the aero-acoustic field, would not have been attained. His happy spirit helped us through many dark hours of computational errors.

The computer resources have been of utter most importance to secure results. A special thanks is thus directed to Chalmers University of Technology.

Finally we would like to thank Seldén Mast. Without their initial idea and interest, this project would not have been possible. William Holt deserves extra acknowledgement for his commitment to the progress of the project.

Jonathan Fahlbeck, Johan Forsgren, Sankar Raju Narayanasamy, Martin Ottosson, David Winqvist, Gothenburg, May 2017

Contents

List of Figures	xi
List of Tables	xi
Nomenclature	xii
1 Introduction	1
1.1 Background	1
1.2 Case Description	2
1.3 Project Goal	2
1.4 Limitations	2
2 Theory	3
2.1 Acoustic Theory	3
2.2 Computational Theory	5
2.2.1 Basics of Fluid Dynamics	5
2.2.2 Basics of Computational Fluid Dynamics	6
2.2.3 Ffowcs Williams-Hawking formulation	6
2.2.4 DNS, LES, RANS, DES	7
3 Method and Computational Settings	8
3.1 Pre-processing	8
3.1.1 Acoustic Domain Setup	8
3.1.2 Mesh generation	9
3.1.3 FW-H Surface and Receivers	11
3.1.4 Mesh Dependency Study	11
3.2 Simulations	12
3.2.1 Boundary Conditions and Material Properties	12
3.2.2 RANS Simulation	12
3.2.3 DES Simulation	13
3.2.4 Stopping Criteria	13
3.3 Post-processing	13
3.3.1 Fast Fourier Transform and Sound Pressure Level	14
3.3.2 Overall Sound Pressure Level	14
3.3.3 λ_2 Criterion	14
3.3.4 Contour Plots	14
4 Results and Discussion	15

Contents

4.1	Velocity	16
4.2	Sound Pressure Level	16
4.3	Overall Sound Pressure Level	17
4.4	λ_2 Criterion and Vorticity.	18
4.5	Additional Results	20
4.6	General Discussion of the Results	21
5	Conclusion	24
	Bibliography	25

List of Figures

1.1	Mast profiles, (<i>a</i>) has a whistling noise, (<i>b</i>) does not have a whistling noise.	1
3.1	Domain and the mast profile (<i>b</i>).	9
3.2	View of a directed volume mesh with 5.6 million cells, for mast (<i>b</i>).	10
4.1	Velocity contour plots.	15
4.2	A-weighted SPL. Data recorded in two receivers. See Figure 4.4 for the location.	16
4.3	PSD of static pressure in the probes located close to the tips. Comparison between the two configurations.	17
4.4	Overall Sound Pressure Level around the two different mast configurations. Note that 0° refers to downstream of the mast.	18
4.5	Isosurface of $\lambda_2 = -250000 \text{ 1/s}^2$, for mast configuration (<i>a</i>) (top) and for mast configuration (<i>b</i>) (bottom).	18
4.6	Vorticity contour plots.	19
4.7	Mast configuration (<i>a</i>).	20
4.8	Vorticity near the mast.	20

List of Tables

3.1	Domain design parameters.	9
3.2	Material data for dry air at 15°C and atmospheric pressure [12].	12

Nomenclature

AA	Aero-Acoustics
ASZ	Acoustic Suppression Zone
CAA	Computational Aero-Acoustics
CFD	Computational Fluid Dynamics
CFL	Courant–Friedrichs–Lewy
CTH	Chalmers University of Technology
DES	Detached Eddy Simulation
DNS	Direct Numerical Simulation
FFT	Fast Fourier Transform
FW-H	Ffowcs Williams-Hawkings
LES	Large Eddy Simulation
OASPL	Overall Sound Pressure Level
PSD	Power Spectral Density
RANS	Reynolds-Averaged Navier-Stokes
SPL	Sound Pressure Level

1

Introduction

1.1 Background

In today's society, people are much concerned about noise pollution. Hence industries strive to make products less noisy in order to comprehend with the awareness and sensitiveness of their customers. The aim of this project is to investigate the unwanted whistling noises created by sailboat masts when the boat is moored and the sail is stowed inside the mast.

An annoying whistling sound may arise when the flow velocity and the yaw angle are large enough in certain boat mast designs. The company Seldén Mast AB desires to know the root cause of this whistling noise in order to enable them to design the masts in accordance to prevent it. Seldén Mast provided Chalmers University of Technology (CTH) with two mast segments, of which one has been experienced to produce a higher noise in comparison to the other. In Figure 1.1 the two mast profiles are illustrated. Since the observations of the whistling sound is based on experiences rather than experimental data the conditions of when this behaviour occurs is not fully known. It has been estimated to a free stream velocity of 20 m/s and a yaw angle from 20° to 45° .

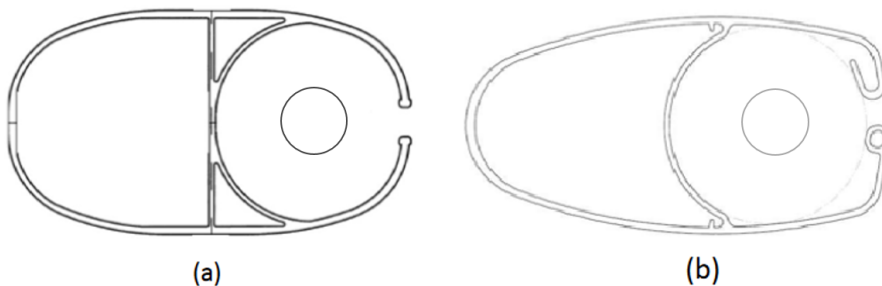


Figure 1.1: Mast profiles, (a) has a whistling noise, (b) does not have a whistling noise.

The aim of this collaboration between CTH and Seldén Mast is to achieve a win-win situation. By using computational fluid dynamics tools, the group at CTH aimed to help Seldén Mast in their understanding on the whistling noise generation. Thereby enabling the company to reduce unwanted sounds generated by the masts and making necessary changes in the design. The proposed analysis of the mast designs will hopefully help the company in making them more competitive. In

addition to the assistance provided to Seldén Mast, the group at CTH intended to improve their skills in project work as well as to enhance their knowledge in fluid mechanics and aero-acoustics.

1.2 Case Description

The two mast configurations in Figure 1.1 are investigated regarding noise generation. Mast (a) has a cross sectional dimension of 148 mm \times 266 mm and mast (b) has a cross sectional dimension of 270 mm \times 140 mm. As noise is generated by turbulence, 3D computations are performed. The height of the two profiles are set to 250 mm, and thus the height of the 3D domain. The flow velocity is 20 m/s and the yaw angle 33°. The fluid is dry air at 15 °C and atmospheric pressure. As 3D computations are challenging, instability issues such as numerical errors, convergence problem and flow field development are expected. Mesh generation is also an area where challenges might be encountered.

1.3 Project Goal

Use acoustic wave modeling to explain the effects of the tip¹ geometry in a mast regarding noise generation. The project should result in recommendations to consider while designing a mast to prevent noise generation.

1.4 Limitations

In order for the project to be feasible within the time frame a number of boundaries and limitations are applied. The project was to be carried out from March to May 2017. The limits are determined by either absolute factors, such as the amount of time available, or in order to assure that an overall quality of the work is attained.

Since unsteady 3D computations was performed, which are both time and computationally demanding, time available and computational resources are of importance. Hence it is hard to establish a fine balance between number of cells and computational time.

The field of aero-acoustics was new for the project group. In the narrow time frame a large amount of the time available had to be used in order to fully understand the underlying problems in the field of aero-acoustics. Thus the task is limited to investigate noise caused by turbulence. Other types of sounds are not to be investigated.

All the simulations are performed in the commercial software STAR-CCM+. The software is also used in the analysis part of the project in combination with MATLAB.

¹The tip geometry refers to the tips at the opening of the mast, see Figure 1.1.

2

Theory

2.1 Acoustic Theory

Acoustics refers to the science of sound and originates from the Greek word for hearing [1]. Sound is of high significance in our every day life when it comes to communication, awareness of our surroundings and orientation. In recent years the awareness of sound and noise has increased. One needs to note that not all sound is bad. We still want to hear a click when we turn the key in the door, music or sounds alerted by warning devices. The sound which today is unwanted is the one that is "out of place" and disturbing [2].

It is known that sharp bangs or long time exposure to loud noises can damage our hearing. In fact noise can also cause other health issues or even death. For example, flies that are exposed to sound levels around 160 dB die after a short period of time. To get this noise level into perspective one can compare this with the noise produced by a refrigerator ~50 dB, a chain saw ~100 dB or a shotgun ~140 dB. Humans who spend much time in areas with loud noise usually have a higher blood pressure and heart rate. Noise has also been proven to affect sleeping patterns and just simply annoys people. All these facts have made companies and whole industries more aware of the effects of noise. Today acoustics is an important aspect in product development [3].

In order to understand how noise travels, one can explain it by looking at what happens when you throw a rock into a lake. When the rock hits the water surface, the rock will be slowed down. The kinetic energy of the rock then is transferred into the water and causes ripples to form on the water surface. The ripples are gradually transported outwards and heating the water slightly as they pass and fade away. In the same way the noise travels from, for instance, a sudden clap of your hands. Energy will spread from the clap in a series of sound waves which consists of regions with increased pressure. The fluid particles will move closer together for a short period of time as the wave passes. For a louder clap, the fluid particles move tighter together and a higher pressure difference is created. Like the ripples on the water, the sound waves of the clap will die away as the energy eventually is transferred into heat. Since the losses are small, sound waves can travel a very long distance before they fade away [2].

There are different ways by which noise or sound can be created. For instance, the one mentioned above which was as a "clap". Others are frictional noise or vibrations

noise from structures. Since the cause of these sounds are fairly straight forward, the industries ability to dampen these sounds has come pretty far. In recent years the removal of the "out of place" sounds has therefore been focusing on other sources of sound such as aero-acoustics. An example of the importance of aero-acoustics is when you are in a car driving at high velocities. If you open the window the aero-acoustic noise will be the dominating one. Aero-acoustic noise generation can in a simple manner be explained by the flow interacting with geometrical irregularities of a car, an airplane, etc. The interaction creates unsteady turbulent flows which are often detached and thus in turn generates noise. The noise generation can be divided into two phenomena: impulsive noise and turbulent noise [3][4].

Impulsive noise is generated by the movement of surfaces or a surface in a non-uniform flow condition. The non-stationary load on the body causes pressure fluctuations to occur, which are generated as sound. This noise can be estimated in a fairly simple manner from aerodynamic simulations. Turbulent noise, on the other hand is harder to predict but it is quite common and predominantly exists. Since the turbulence is stochastic by nature, it has a broad frequency spectrum. The turbulent noise therefore creates a broadband noise consisting of many frequencies. Turbulent energy is most efficiently transferred into acoustic energy in the presence of sharp edges. The sharp edge forces two flows of different velocities to have a sudden blend. An example of this is when a flow crosses a bluff body. Unless the body is aerodynamically shaped the fluid will separate from the body and cause a wake to form behind the body. The wake will consist of fluid with low velocity. The pressure difference between the still fluid and the fluid crossing the body will cause them to blend. This causes strong local equalizing flow which in turn results in peak pressures, i.e impulsive noise. Behind a bluff body the pressure will characteristically alternate to the different sides of the wake in order to comprehend with the velocity of the moving flow on both sides of the wake. This effect is a Von Kármán vortex street which refers to the fluid twirls of alternating directions forming behind an object. Vortex shedding is the phenomenon of every fluid twirl "coming loose" from the body [3][5].

As stated in previous paragraph, vorticity is generated at boundaries by the relative velocity of two surfaces, such as fluid and wall. When a certain threshold is reached the two-dimensional wakes formed by vorticity, shed from the bluff body surface. This results in a transition into the third dimension. The feature explains the fact that the vorticity can be stored as a vortex street, leading to conservation of vorticity in a system. Since the vorticity is mainly created just downstream of a bluff body the vorticity further downstream is merely a response of the rest of the fluid, trying to adjust to the instability that the bluff body initialized. Vortices tend to merge downstream of the bluff body, creating larger sections of rotating fluid with lower velocity. As a result one could state that the vorticity generated immediately downstream of the bluff body is of higher importance [6].

Since turbulent broadband noise always exists when turbulence is present, one can state that Aero-Acoustic (AA) noise consists of a broadband noise. Sometimes it is

accompanied by a narrow-band impulsive noises. As previously stated, though the impulsive noise is fairly easy to predict, in order to predict the turbulent noise one has to estimate the turbulence. Hence, in order to fully estimate the AA noise one has to use CFD-tools. This is a fairly recent methodology that has been evolved with the utilization of computers. This field of science is called Computational Aero-Acoustics (CAA) [3][4].

There are two main methodologies in CAA to compute an acoustic field. The first one being "direct method", which is considered to be the most exact and would be the equivalent to DNS in the CFD field. In the direct method the governing equations for the flow and acoustic field are solved over the entire domain, from the aerodynamic effective area to a far-field observer. The fact that the domain of interest is very large, makes the direct method extremely expensive when it comes to the number of cells and time steps. The more common way to perform AA computations is to use hybrid methods. The sound generation in the aerodynamic effective area is decoupled from the transport of the sound to the far-field. In more simple terms one can say that one method is used for the sound generation and another method is used for the transport process. There are several methods available, both for sound generation and the transport process [3].

Even though the possibility to fully estimate the aero-acoustic noises is fairly new due to improvement in technology (computers) today, a lot of the ground work was performed in the 1960s. Many of the equations still used today are based on the acoustical transport techniques from half a century ago. The most frequently mentioned ones are the Lighthill analogy and the Ffowcs Williams–Hawkings (FW-H) equation. These are used as transport methods while performing calculations with the hybrid techniques [3]. The FW-H equation is explained in the section 2.2.3.

2.2 Computational Theory

In order of fully understanding CAA some basic principles need to be addressed. As stated in section 2.1, CAA is a mixture of acoustic theory and CFD. In this chapter the theory behind these aspects will be explained. The aim is that this chapter will help the reader in the understanding of the final results.

2.2.1 Basics of Fluid Dynamics

The principle of fluid dynamics is that it describes a pattern of flows. In fluid mechanics it is common to investigate a flow within a fixed control volume. The flow is governed by the continuity (eqn 2.1), Navier-Stokes (eqn 2.2) and energy (eqn 2.3) equations [7].

$$\frac{d\rho}{dt} + \rho \frac{\partial v_i}{\partial x_i} = 0 \quad (2.1)$$

$$\rho \frac{dv_i}{dt} = -\frac{\partial p}{\partial x_i} + \frac{\partial}{\partial x_j} \left[\mu \left(\frac{\partial v_i}{\partial x_j} + \frac{\partial v_j}{\partial x_i} - \frac{2}{3} \frac{\partial v_k}{\partial x_k} \delta_{ij} \right) \right] + \rho f_i \quad (2.2)$$

$$\rho \frac{du}{dt} = \sigma_{ij} \frac{\partial v_i}{\partial x_j} - \frac{\partial q_i}{\partial x_i} \quad (2.3)$$

Here ρ is density, v velocity, x length, t time, p pressure, u internal energy, q conductive heat flux, f body force and σ the stress tensor.

2.2.2 Basics of Computational Fluid Dynamics

In CFD the variables of a flow field are solved for inside a domain of interest using a computational software. The domain is discretized into a number of finite volumes or cells in which the governing equations are solved in an iterative process. Depending on the type of flow, different numerical schemes are used to discretize the differential equations.

2.2.3 Ffowcs Williams-Hawking formulation

This formulation is a more general form of Lighthill's equation [8][9], where moving walls are allowed to be present inside the domain. The formulation is based on the assumption that a volume $B(t)$ exists which is enclosed by the surface $S(t)$. The surface needs to be sufficiently smooth to allow the definition of a smooth function $h(\mathbf{x}, t)$ such that

$$h(\mathbf{x}, t) = \begin{cases} > 0 & \text{if } \mathbf{x} \in B(t) \\ = 0 & \text{if } \mathbf{x} \in S(t) \\ < 0 & \text{if outside } B(t). \end{cases}$$

One can note that the Heaviside function of this function, $H(h)$, will be zero inside the volume $B(t)$ and unity outside $B(t)$. If the mass conservation equation and momentum equation is multiplied by $H(h)$, use Lighthill's procedure for acoustic variable, $p' = p - p_0$, apply Green's theorem and use the free-space Green's function, equation 2.4 can be obtained [3].

$$\begin{aligned} p'(\mathbf{x}, t) = & \frac{\partial^2}{\partial x_i \partial x_j} \int_{\mathbb{R}^3} \left[\frac{(\rho v_i v_j - \sigma_{ij}) H}{4\pi r} \right]_{\tau=t_e} dV_y - \frac{\partial}{\partial x_i} \int_{\mathbb{R}^3} \left[\frac{\mathbf{f} H}{4\pi r} \right]_{\tau=t_e} dV_y \\ & + \frac{\partial^2}{\partial t^2} \int_{\mathbb{R}^3} \left[\frac{(p'/c_0^2 - \rho') H}{4\pi r} \right]_{\tau=t_e} dV_y \\ & + \frac{\partial}{\partial t} \int_{S(t_e)} \left[\frac{\rho_0 \mathbf{b} \cdot \mathbf{n}}{4\pi r(1 - M_r)} \right]_{\tau=t_e} dS - \frac{\partial}{\partial x_i} \int_{S(t_e)} \left[\frac{p' n_i - \sigma_{ij} n_j}{4\pi r(1 - M_r)} \right]_{\tau=t_e} dS \end{aligned} \quad (2.4)$$

σ_{ij} is the viscous stress, n is the normal to the surface, $H = H(h)$, $r = \|\mathbf{x} - \mathbf{y}\|$, \mathbf{f} is the body force, c_0 is the speed of sound in the fluid surrounding the listener, \mathbf{b} is the velocity of the moving surface, $M_r = \mathbf{b} \cdot (\mathbf{x} - \mathbf{y}) / rc_0$ and $t_e = t - r/c_0$.

The two surface integrals in equation 2.4 are later used to set up the FW-H surface integral as equation 2.5. See section 3.1.3 for further information.

$$p'(\mathbf{x}, t) = \frac{\partial}{\partial t} \int_{S(t_e)} \left[\frac{\rho_0 \mathbf{b} \cdot \mathbf{n}}{4\pi r(1 - M_r)} \right]_{\tau=t_e} dS - \frac{\partial}{\partial x_i} \int_{S(t_e)} \left[\frac{p' n_i - \sigma_{ij} n_j}{4\pi r(1 - M_r)} \right]_{\tau=t_e} dS \quad (2.5)$$

2.2.4 DNS, LES, RANS, DES

The major models that are utilized for solving turbulence in CAA or CFD as a whole are Direct Numerical Simulation (DNS), Large Eddy Simulation (LES), Reynolds Averaged Navier-Stokes Simulation (RANS) and Detached Eddy Simulation (DES) [7].

DNS solves all the turbulence scales, making it highly expensive. Thus it is not suggested to be performed for objects with larger dimension with the computational facilities currently available.

LES resolves all large turbulent scales, i.e, it is volume averaged. The principal idea behind LES is to reduce the computational cost by modelling or exclude the smallest scales, which are the most computationally expensive to resolve. This is achieved via averaging across time and space, which effectively removes small-scale information from the numerical solution.

RANS models all turbulence. It is time-averaged and different turbulence models are applied. Thus making it faster than other methods to compute. The most common turbulence models are the $k - \varepsilon$ or $k - \omega$.

DES is a combination of advantages of both RANS and LES. In DES, the scales close to the wall are solved using RANS (or unsteady-RANS), within the boundary layer. Further away from walls are the scales resolved using LES. Thus DES behaves as a hybrid RANS-LES model.

3

Method and Computational Settings

While performing the analysis of the two mast designs a methodology divided into three stages was used. The different stages were Pre-processing, Simulation and Post-processing. Most of the work was performed in the commercial software STAR-CCM+. The work was initially performed on mast profile (a) (see Figure 1.1) due the simplicity of the geometry. All through the process, thorough documentation of the choices made were performed. This was later used when repeating the set up for mast (b). In this fashion a precise comparison between the two designs could be established.

3.1 Pre-processing

When performing analysis using numerical methods, the quality of the final result is highly dependent of the work done prior to pushing the "run button". A well planned domain using a suitable mesh design to account for the important features is therefore crucial. In this section the different parts of the Pre-process will be explained.

3.1.1 Acoustic Domain Setup

The outer domain design was based on the mast mean diameter D_m . In Figure 3.1 and in Table 3.1 the design features are visualized. The principle of the design in Figure 3.1 is that the white area (outer domain) is formed by a coarser mesh while the gray area (inner domain) has a finer mesh. This feature was applied in order to capture the small-scale flow structures downstream of the mast. The bold line which is dividing the areas is a FW-H surface, see section 3.1.3. A RANS simulation was performed and gave a good estimation of the size and location of the turbulent flow field behind the mast. This simulation was used to define the gray shaded refinement zone and the FW-H surface.

In general is it necessary to use a very large domain when numerically calculating acoustics. This is because the pressure fluctuations that noise is built from are small and therefore sensitive to disturbance. Any presence of reflected noise could affect the result. The following methods were used to reduce the risk of reflecting noise and numerical errors:

- To reduce the reflections of sound with high frequency an increased cell size near the boundary was used. This makes the mesh unable to capture the

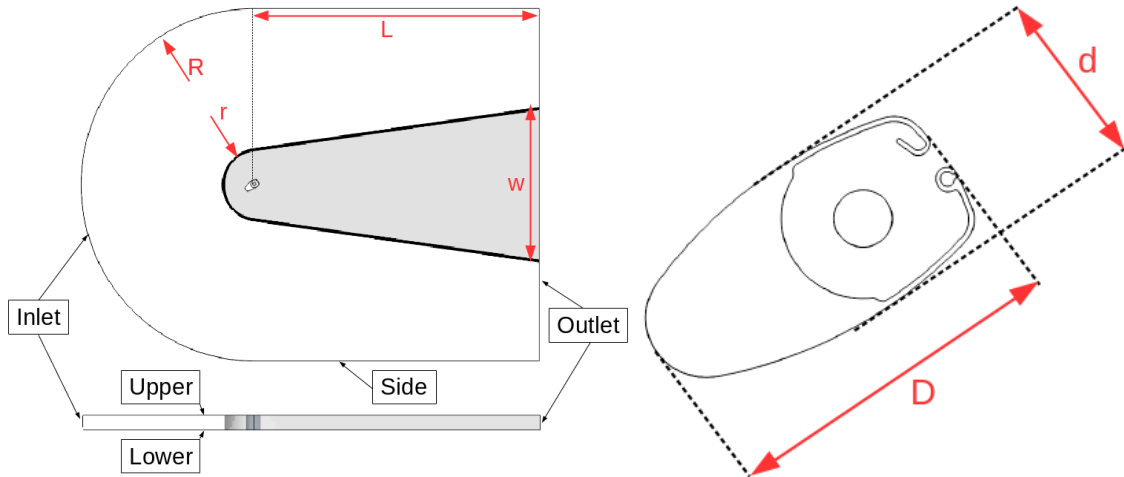
sounds since approximately 20 cells per wavelength is needed to capture the sound correctly [10]. This design also has the advantage that it reduces the computational effort.

- Regarding the sound with low frequency an acoustic Suppression Zone (ASZ) was used around the boundary. ASZ dampens the acoustic waves before they reach the outer boundaries to prevent them from reflect back into the domain. The zone can therefore be thought of as a sponge absorbing the sound. The zone size, l , could be estimated from the speed of sound, c_0 , and predicted minimum frequency, according to equation 3.1.

$$c_0 = 340 \text{ m/s}, \quad f_{\text{minimum}} = 500 \text{ Hz} \Rightarrow \quad l = \frac{c_0}{f_{\text{minimum}}} = 0.68 \text{ m} \quad (3.1)$$

Table 3.1: Domain design parameters.

Parameter	D_m	R	L	r	w	D	d
Used size	$(D + d)/2$	$15D_m$	$25D_m$	$3D_m$	$13D_m$	0.27 m	0.14 m



(a) Domain seen from above (top) and from (b) Illustration of mast profile (b), the side (bottom). with geometrical lengths.

Figure 3.1: Domain and the mast profile (b).

3.1.2 Mesh generation

In order to find a suitable mesh for performing the simulations, a couple of parameters needed to be taken into account. Firstly, the mesh should not exceed more than 10 million cells. This was to ensure that the computational resources provided were used effectively. Secondly, the mesh needed to be fine enough in the areas where small-scale vortex shedding occurs. This is where sound generation is expected. The main areas of interest were the region around the tips (Figure 3.2c) and the region behind the mast (Figure 3.2b). The mesh in these regions was controlled by a wake

refinement operation. Here one could specify the direction of the anticipated flow, to which the geometry will be exposed. The length, angle and the cell growth rate of the zone were controlled. The mesh can be seen in Figure 3.2.

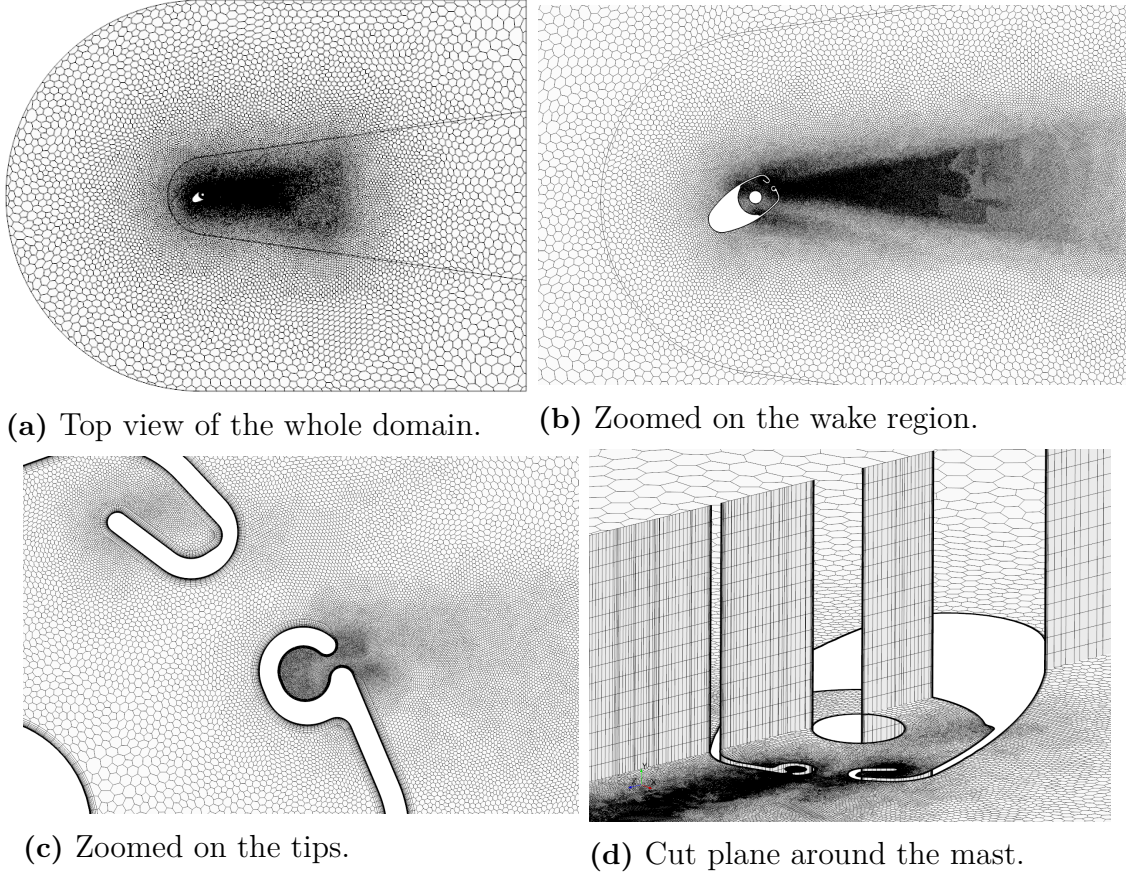


Figure 3.2: View of a directed volume mesh with 5.6 million cells, for mast (b).

To properly resolve the acoustics, the cell size must be small enough. One good practise in estimating the cell size is to use the fact that at least 20 cells per wavelength is preferable [10]. With the speed of sound, estimated to be the standard value at sea level, $c_0 = 340$ m/s, combined with an approximate value for what the frequency of the noise might be, $f_{whistling} \approx 1000$ Hz, the cell size can then be calculated according to equation 3.2.

$$\Delta_{CAA} = \frac{c_0}{20f_{whistling}} = 0.017 \text{ m} \quad (3.2)$$

This cell size was desirable to transport the sound correctly in the inner domain. In section 3.1.1 a couple of ways to minimize the risk of reflected noise are listed. These strategies were included into the mesh.

In addition to the mesh design in regards where to have large/small cells, the actual mesh design needed to be accounted for. In 3D simulations, as in this case, three common mesh types are tetrahedral, hexahedral and polyhedral. Tetrahedral is the least complex with four vertices, four faces and six edges. The other ones are more

complex and are built from several tetrahedral cells. This results in the tetrahedral mesh being the fastest to generate, but lacks in accuracy when solving the actual problem, since the error decreases as the number of cell faces increases. In acoustic simulations, a large number of iterations is in general required in order to attain a correct solution. Therefore, even though the mesh takes longer time to generate, the polyhedral mesh was the most suitable candidate, due to a higher accuracy at a shorter computational time.

The whole mesh generation process was performed in an iterative manner where different mesh strategies were tested. Methods that were tested and later discarded were for example mesh designs using volumetric control for the entire domain, another one using surface controls. The finally chosen mesh generation method was a directed mesh. The advantage of this strategy is that the mesh is easy to control regarding number of cells. The mesh is also faster to compute in comparison to the other used methods. The fact that this thesis aims to compare two different geometries was an argument for the choice of an easily controlled mesh and thus the directed mesh.

3.1.3 FW-H Surface and Receivers

In order to capture the noise generated by the mast, a permeable FW-H surface was applied within the computational domain. The data from CFD computations were then extracted along the FW-H surface as suitable source terms in the acoustic equations [11], see section 2.2.3 and equation 2.5.

The FW-H surface was applied as an internal interface between inner and outer region within the fluid domain, see bold line in Figure 3.1. Once AA had been enabled in the used software, the interface was treated as a permeable surfaces within the "FW-H surface" menu.

A number of FW-H receivers (36) was adopted outside of the fluid domain to record the acoustic data. The receivers were installed in a circular pattern, with a radius of 10 m, around the mast. Since the acoustic transport equations are decoupled from the flow equations it is possible to place the receivers outside of the domain.

3.1.4 Mesh Dependency Study

A mesh dependency study is planned in order to establish mesh independent results. It is desirable to find a mesh giving accurate results without wasting computational resources.

The study was planned so that the general design of the mesh were unchanged and the only difference was the number of cells. Three different meshes were created for mast configuration (a) (see Figure 1.1) with 2.2, 4.4 and 7 million cells. Probes were inserted into the domain to measure velocity and pressure to later be able to compare the results. The plan was then to choose one mesh and apply this

set up also for mast configuration (b). Unfortunately problems were encountered regarding finding a converged solution. A lot of time was spent on fixing this and when a converged solution was obtained the time was too short to analyze all the meshes. Therefore, a fully completed mesh dependency study was not performed. For the final results, a 4.4 million cell mesh and a 5.6 million cell mesh were used for mast configuration (a) and mast configuration (b), respectively. The difference in cell number between the mast configurations is due to varying complexity in the geometry.

3.2 Simulations

This section consists of different settings and options used for the simulations in STAR-CCM+. The settings and preferences used in all simulations are based upon [10], discussions with supervisor and the project group.

3.2.1 Boundary Conditions and Material Properties

The names of the domain boundaries can be found in Figure 3.1. The Inlet boundary was set as a velocity inlet with a laminar incoming flow. Sides and Outlet were set as pressure outlet. Atmospheric pressure at sea level was prescribed for the pressure outlets. The Upper and the Lower boundaries were set to periodic boundary condition where the flow propagates from one boundary to the other.

The fluid is dry air at 15 °C and atmospheric pressure (101325 Pa). Other material properties under consideration are presented in Table 3.2. The ideal gas law is a viable assumption for the cases investigated. It is a fair approximation, since the regular air at non-extreme temperatures and pressure are used in these simulations.

Table 3.2: Material data for dry air at 15 °C and atmospheric pressure [12].

T [K]	ρ $\left[\frac{\text{kg}}{\text{m}^3}\right]$	μ $\left[10^{-6}\frac{\text{N}\cdot\text{s}}{\text{m}^2}\right]$	κ $\left[10^{-3}\frac{\text{W}}{\text{m}\cdot\text{K}}\right]$	C_p $\left[\frac{\text{J}}{\text{kg}\cdot\text{K}}\right]$	Pr
288	1.226	17.96	25.24	1006	0.7159

T temperature, ρ density, μ kinematic viscosity, κ thermal conductivity, C_p specific heat capacity, Pr Prandtl number.

3.2.2 RANS Simulation

Initially a RANS simulation was performed to understand the turbulent flow field around the mast. This simulation was performed to get an initial solution, from which a more comprehensive DES simulations could be performed, see section 3.2.3. The RANS simulation was performed as a steady state simulation using segregated flow solver but without any AA features. The SST $k - \omega$ model was used together with all y^+ wall treatment. During the RANS, first order schemes were used so that a solution for the flow field could be attained rapidly.

3.2.3 DES Simulation

DES and AA tools were utilized in order to find and determine the source of the noise. The initial solution was obtained from the steady state RANS simulation. In contrast to the RANS the DES was carried out with an implicit unsteady scheme where a low CFL number was desirable. A Segregated flow solver was applied, just as for the RANS. The utilized model was SST $k - \omega$ with all y^+ wall treatment enabled. In the DES, second order schemes were used to achieve a higher accuracy. The convection was treated with a Hybrid-BCD scheme.

During DES, the number of iterations per time step was used as an important factor to govern the over all convergence. It is critical to attain convergence within every time step and then consequently convergence in time as well. The number of iterations per time step was set to 10 due to promising convergence while monitoring the residuals.

To develop the correct unsteady behaviour in the flow field the fluid needs to pass through the domain several times. In practice this meant that two different options could be used. Either the simulation needed to go on for a long time, which would be expensive regarding computational power. Another alternative is to start at a large time step and develop the field and then gradually decreasing it until a sufficiently low time step is reached. The second option was used during this project. The time step was first set to 10 ms and then decreased in several steps to a final time step of 0.1 ms. The final time step gave a maximum CFL number of around 10. This was considered the lowest possible time step due to the computational power available and was therefore good enough for this project.

The enabled acoustic options were "FW-H unsteady", along with an Acoustic Suppression Zone (ASZ). The FW-H was used with the "On-the-fly" model option which provides noise prediction in the receivers in parallel with the CAA. The Inlet, Sides and Outlet boundaries had the ASZ set to 0.68 m. At the other boundaries no ASZ was applied. The ASZ was configured to suppress low frequencies since high frequency is dampened by increasing cell size near the boundaries, see Section 3.1.1.

3.2.4 Stopping Criteria

The stopping criteria were based on residual plots, monitor plots and receivers in the far field. It was of importance to let the simulation run for sufficiently long time for the receivers to capture enough noise data.

3.3 Post-processing

In the Post Processing stage, the focus is to analyze the gathered data. This section explains the methods of comparison when analyzing the wind induced noise level for the different masts.

3.3.1 Fast Fourier Transform and Sound Pressure Level

For analyzing the aero-acoustics, a Fast Fourier Transform (FFT) algorithm was used to process the signals recorded by the receivers. The receivers record the pressure fluctuations over time and the FFT algorithm transforms the time dependent signals from the time domain into the frequency domain. After the FFT the Sound Pressure Level (SPL) was plotted as function of frequency to distinguish tonal peaks in the signal. This operation was efficiently performed using an FFT tool in STAR-CCM+. The SPL was calculated using the A-weighting function. This means that low frequency noise is filtered out in the similar way as in the human ear.

In order to analyze if the noise recorded in the receivers was generated from vortex shedding produced by the tips of the masts, probes were introduced in these areas to monitor the static pressure. An FFT algorithm computation was then performed on the pressure-time history from the probes. This procedure was similar to that of the data obtained from the receiver. The difference is that instead of the SPL, the Power Spectral Density (PSD) was computed. PSD describes the signal power per unit frequency. To confirm if the sound originates from this region, the pressure spectra from the receivers and that of the probes should be of similar pattern. If a pressure peak is present in the SPL from the receivers, a similar peak should appear in the PSD from the probe data. This would imply that the noise is generated in the region of the probe.

3.3.2 Overall Sound Pressure Level

In order to visualize the direction in which the highest level of noise is produced, the Overall Sound Pressure Level (OASPL) was computed in every receiver location. The OASPL is based on the root mean square value of the pressure fluctuations. MATLAB was utilized for these calculations.

3.3.3 λ_2 Criterion

The λ_2 criterion is a technique that was utilized to visualize the vortices in the turbulent flow using isosurfaces. An isosurface is a surface in space where a certain variable is constant, in this case λ_2 . This method utilizes the eigen value of the strain rate tensor, S and vorticity tensor, Ω . λ_2 is then the median eigenvalue from $S^2 + \Omega^2$, i.e. $\lambda_1 \leq \lambda_2 \leq \lambda_3$ [13] [14]. Hence it was of interest to investigate λ_2 , as the vorticity produced in the wake region is known to have a strong correlation to the generation of noise.

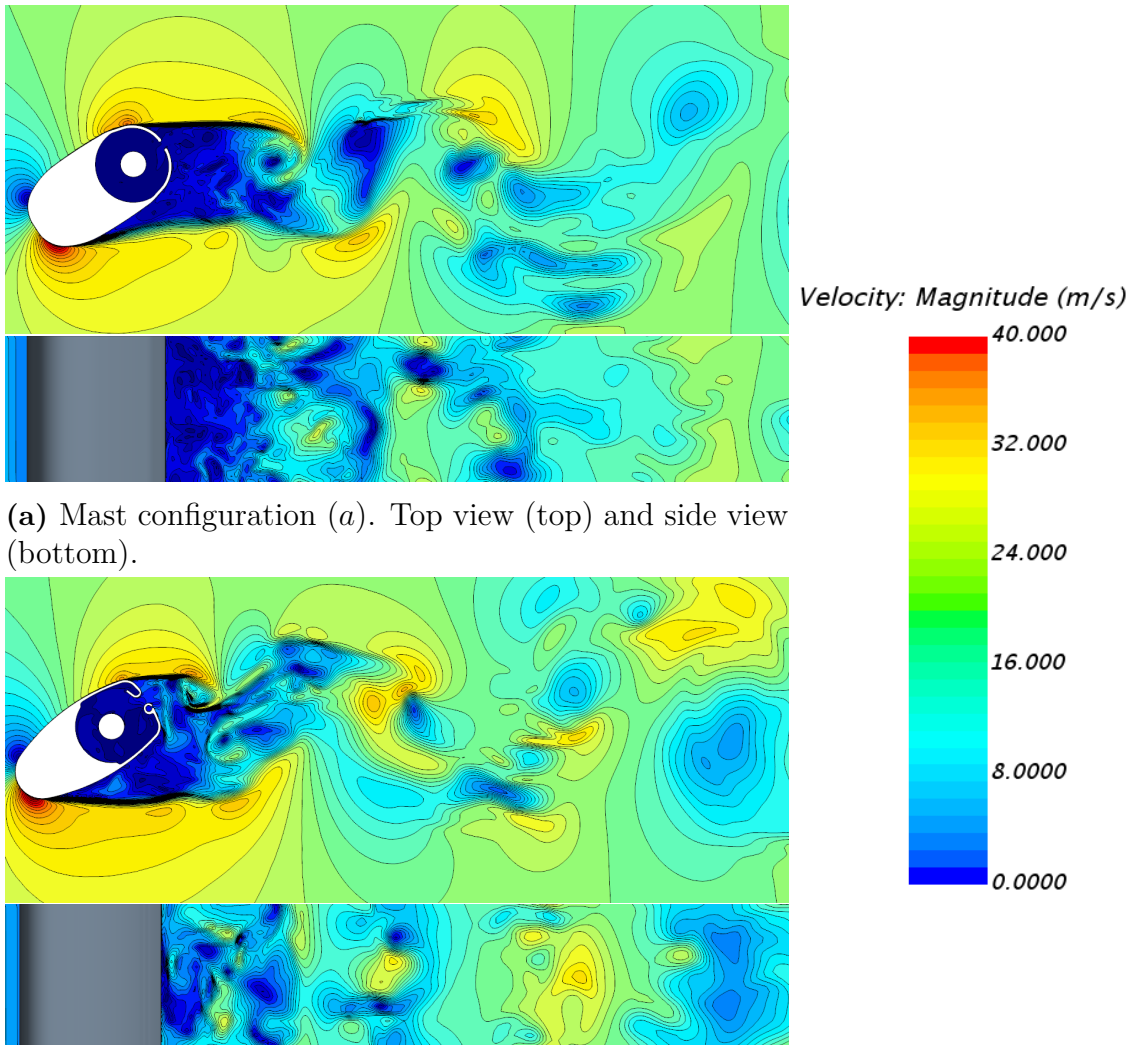
3.3.4 Contour Plots

Velocity plots were utilized to visualize the flow field. It was important to analyze the vorticity contour plots, as they depict the vortex shedding which is correlated to noise generation.

4

Results and Discussion

This chapter presents the results and the discussion of those. To simplify the understanding of noise generation, the flow field is discussed first. Gradually the various physical aspects of noise generation are presented and analyzed. The results are based upon the 4.4 million mesh for mast (a) and a 5.6 million mesh for mast (b).



(a) Mast configuration (a). Top view (top) and side view (bottom).

(b) Mast configuration (b). Top view (top) and side view (bottom).

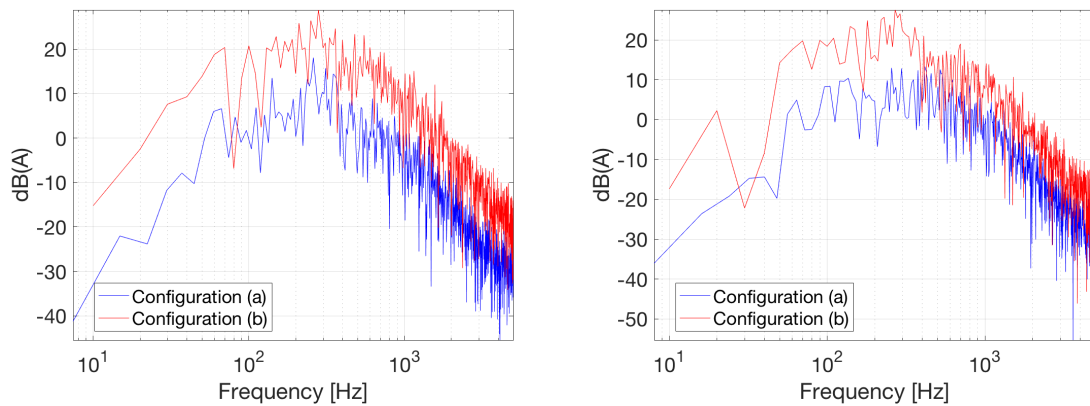
Figure 4.1: Velocity contour plots.

4.1 Velocity

To get a better understanding of the flow field around the masts, the velocity contour plots are shown in Figure 4.1. As expected, the flow fields look similar for both configurations. A wake pattern has been formed downstream of the mast and shows a Von Kármán vortex street. The vortex street is caused by the unsteady flow separation. From Figure 4.1 one could see that the vortices in the wake are created from the bluff body and not from the tip geometry. Mast configuration (b), which was not expected to create a high level of noise, also seems to create a larger unsteadiness than mast configuration (a). This indicates that mast configuration (b) should produce a higher level of noise than mast configuration (a), according to the theory in section 2.1.

4.2 Sound Pressure Level

As stated in section 2.1, the noise consists of a turbulent and an impulsive part. The turbulent noise is often referred to as broadband noise and consists of noise in several frequencies. This project has been aimed to investigate the source of the tonal noise which originates from the impulsive noise. In Figure 4.2 an FFT has been performed on the pressure-time data from the receivers and is presented as an A-weighted SPL. The spectra for both mast configurations show a broadband noise without any obvious protruding peaks, indicating that no tonal noise can be observed. The graphs show that the SPL for configuration (b) is higher than for mast geometry (a). Although, the sound pressure levels are considered to be relatively low.



(a) Receiver at 90° .

(b) Receiver at 270° .

Figure 4.2: A-weighted SPL. Data recorded in two receivers. See Figure 4.4 for the location.

In order to evaluate the origin of the noise, probes were deployed in the domain for data comparison with the receivers. The location of the probes can be seen in Figure 4.3a. In this case the receivers do not indicate any tonal noise generation. In order to verify if this result is correct, it is possible to look at the pressure fluctuations

in the probes, see Figures 4.3b, 4.3c and 4.3d. Here it can be seen that no obvious spectral peaks occur. Hence it is possible to state that the recordings in the receivers are reliable and no tonal noise is created in any of the mast configurations.

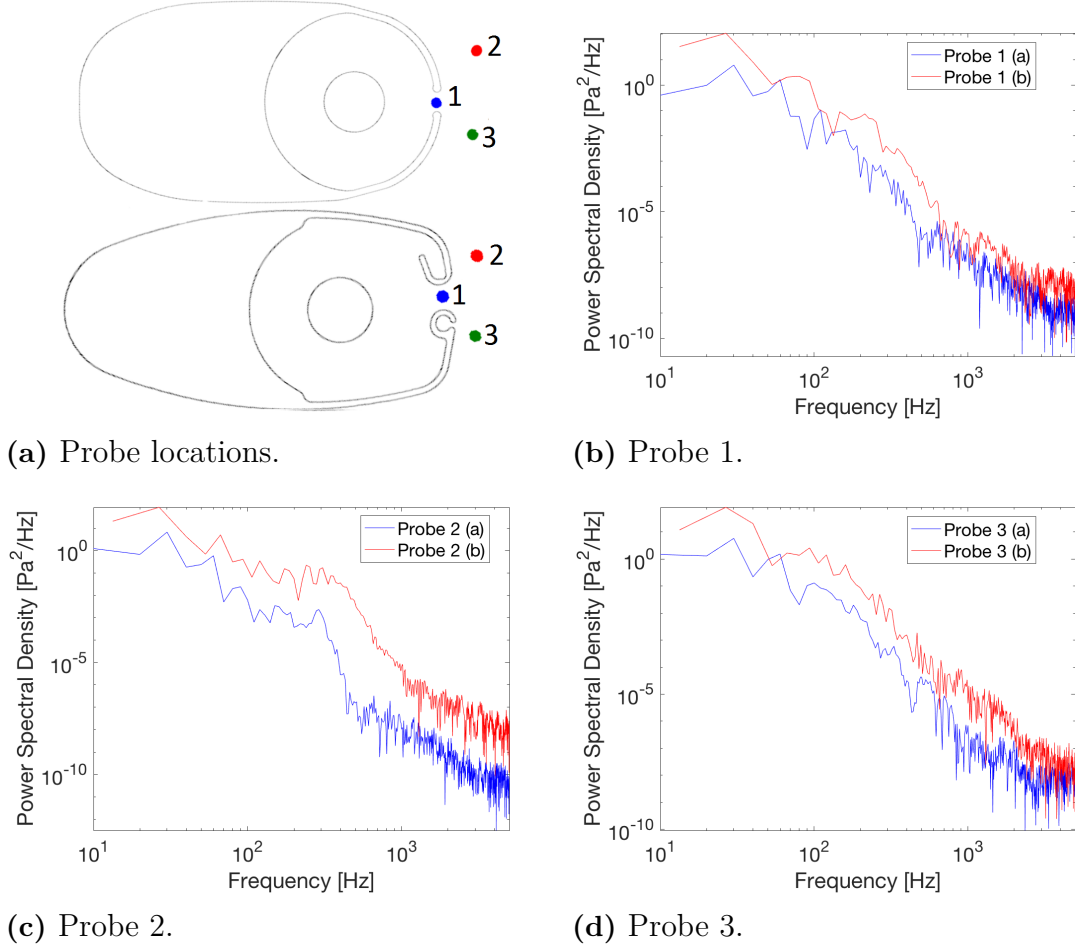


Figure 4.3: PSD of static pressure in the probes located close to the tips. Comparison between the two configurations.

4.3 Overall Sound Pressure Level

The Overall Sound Pressure Level for both mast configurations can be found in Figure 4.4. The Figure is oriented as such that the inflow comes from the left hand side (180°). The Figure shows the OASPL in each of the 36 receivers deployed around the mast. The shape of the noise profile is similar for both the cases. The highest noise is found diagonally downstream of the mast. The lowest noise is found upstream of the mast, which is reasonable as the mast is blocking the sound which is created in the wake. It is also evident that the sound level is higher for mast configuration (b).

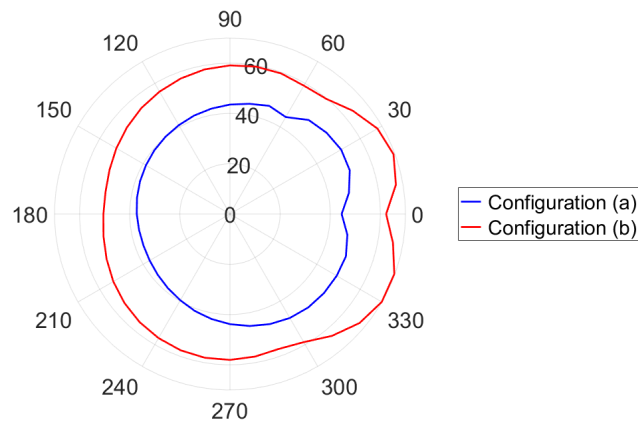


Figure 4.4: Overall Sound Pressure Level around the two different mast configurations. Note that 0° refers to downstream of the mast.

4.4 λ_2 Criterion and Vorticity.

The λ_2 criterion is visualized for the two mast configurations in Figure 4.5. As can be seen mast (b), contradictory to real world experience, generate an intenser vortex shedding than (a) near the tips. Thus it could be claimed that mast configuration (b) will generate a larger noise at this yaw angle. Also in this visualization it can be seen that vortices seems to be created from the mast body and not from the tips. This gives a hint that, for this case, the tips do not generate vortex shedding and thus hardly a tonal noise, according to the theory.

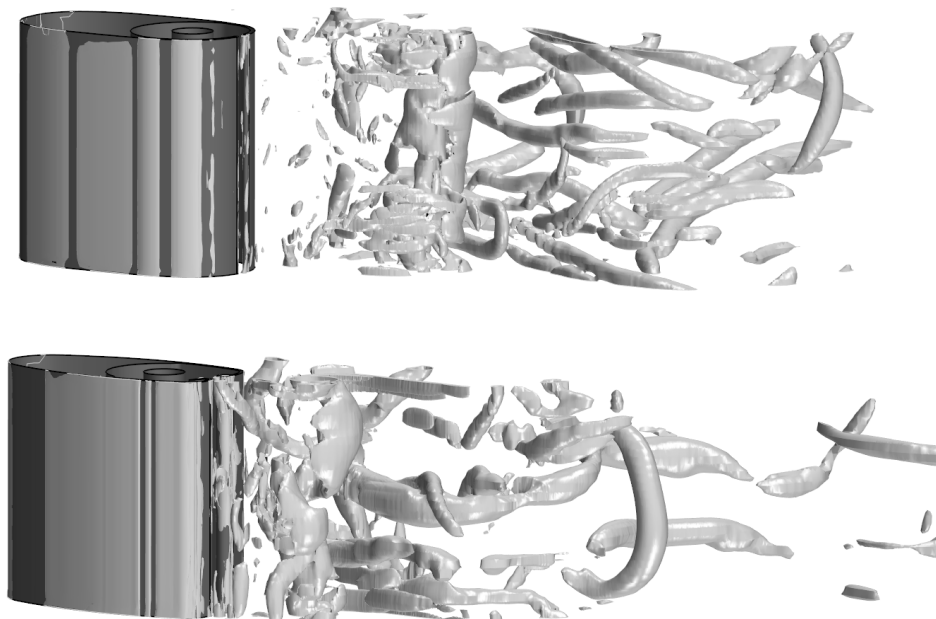


Figure 4.5: Isosurface of $\lambda_2 = -250000 \text{ 1/s}^2$, for mast configuration (a) (top) and for mast configuration (b) (bottom).

The vorticity contours, see Figure 4.6, show that the mast (b) generates stronger vorticity than configuration (a) near the tips. As vorticity is a good indicator of noise, one could claim that configuration (a) produces less noise compared to mast (b). Also, it could be found that the generation of vorticity is largely governed by the bluff body, rather than the tips at this angle of attack.

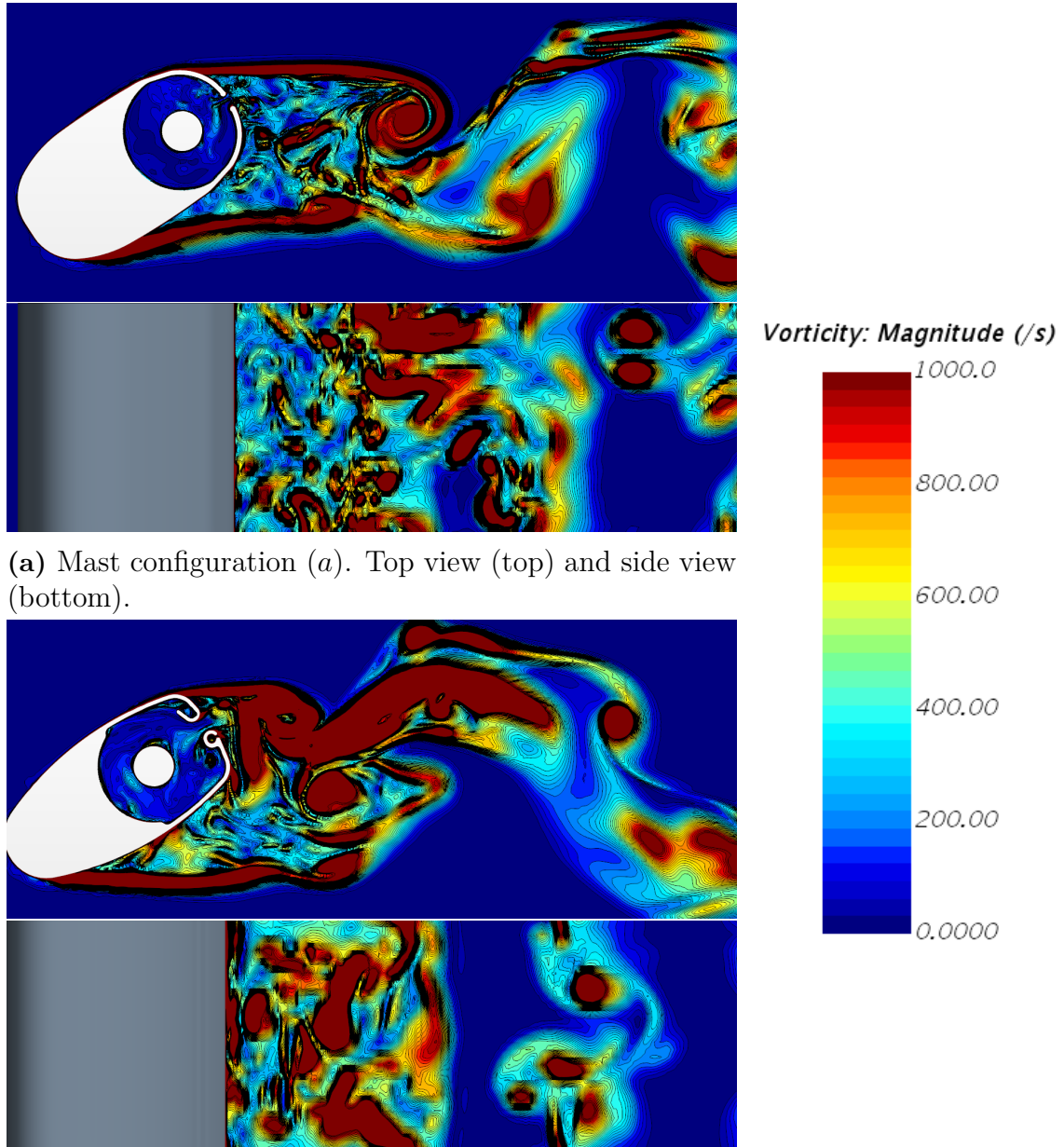


Figure 4.6: Vorticity contour plots.

By both the visualization of the vorticity in Figure 4.6 and the λ_2 -criterion in Figure 4.5 one can see that major vorticity occurs near the mast for the (b) case and not in (a). This could be some indication of that vortex interaction with the tips of configuration (b) will not create any tonal noise, since the interaction occurs but the mast still not produces any tonal noise according to Figure 4.2. For configuration (a) nothing about the correlation between vortex interaction with the tips and tonal noise can be stated, since the vortices are completely separated from the tips.

4.5 Additional Results

While the project progressed, several different simulations were performed. Due to the low rate of acoustic simulation experience, many of these simulations were in purpose of practice. Consequently the results from the simulations have been of varying quality. During this period of trial and error a few interesting findings have been made. The results from using an initial coarser mesh with 2 million cells, showed signs of producing more noise than the final result. It is of importance to note that due to the mesh being more coarse, these results cannot fully be trusted. Nevertheless a few interesting details can be observed. In Figures 4.7-4.8 a comparison has been made between an initial result for a coarse mesh and the final result. The sound pressure level for the two meshes can found in Figure 4.7. In Figures 4.8a and 4.8b the vorticity is plotted close to the tips for both meshes respectively. As previously stated in section 2.1, noise and vorticity does in theory have a strong correlation. It can be seen in Figures 4.7-4.8 that the higher sound pressure level coincides with a higher degree of vorticity around the tips of the mast.

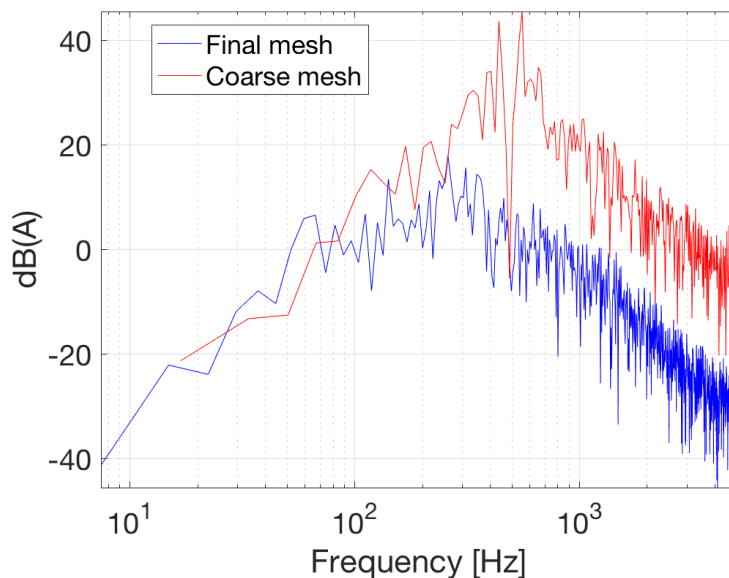
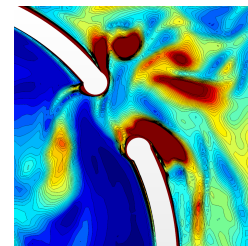
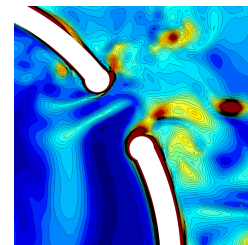


Figure 4.7: Mast configuration (a).



(a) Coarse mesh.



(b) Final mesh.

Figure 4.8: Vorticity near the mast.

4.6 General Discussion of the Results

To summarize the results, it is found that mast configuration (b) generates a higher noise level than (a). This is in contrast to what was expected from real life observations. According to Seldén Mast the noise from mast (a) should be louder than the noise from mast (b). No significant tonal noise has been recorded during the simulations. The only noise that has been captured is broadband noise. The captured noise level has also been very low, approximately 20 dB.

It is of interest to evaluate why the sound levels found in the simulations do not coincide with the expectations. A topic of interest is the angle of attack which is evaluated. This angle is set to be 33° . As stated previously, it does not look like the vorticity reaches the tips of the mast (a). From the observations made prior to the project it was expected that the noise was occurring when the flow was coming in at an angle of attack of around 20° - 45° . If another angle of attack had been examined, the results might have differed.

A source of error could be that in real life the flow is never laminar. There is always turbulence and fluctuations in the wind. In the presence of turbulent flow, the separation of the flow occurs at a later stage from the surface of the bluff body. This would perhaps convey the fact that the vortices would be created closer to the tips of the mast. Hence the tips of the mast would be exposed to larger pressure fluctuations and noise would be generated. The delayed separation in combination with the fluctuating wind direction would imply that the noise generation in real life is less sensitive to the angle of attack in regard with the simulated case.

It is of interest to discuss why there is a difference in result between the initial solution with 2 million cells and the final result for configuration (a). It would have been of great interest to perform a full mesh dependency study. Due to lack of time, this could not be done and hence both results are interesting to discuss. The mesh was in both cases performed in a very similar fashion and the only difference is the number of cells, which were 2 million and 4 million. The difference in cell size is therefore two times in volume, but regarding the length of one cell this results in a difference of $2^{1/3}$ which is hard to visualize graphically. The first possible reason for the difference in result between the two meshes is that the coarser mesh is simply not fine enough and hence the faulty results are found. Another one could be that due to the size of the mesh, the coarser one ran for a longer time. Hence the flow could be picked up at a later time step. There is a possibility that the final mesh for configuration (a) has not yet reached the time where the vortices occur close behind the mast. Perhaps the most likely reason is that due to the perfect case of laminar flow that hits the mast, the finer mesh resolves this very well and a large wake is created that never gets close to the tips. The coarser mesh on the other hand does not solve the flow as well and there is an error that causes the vorticity to occur close to the mast. Interesting to note here is that to some extent the reason for the vortices acting close behind the mast is of less importance. By using the result from the coarser mesh we can discuss what would happen if the vortices actually

did effect the tips.

In section 4.5 it was shown that the initial results with a coarse mesh gave a higher SPL than the final results. Here the correlation between SPL and vorticity could be studied. The fact that more noise is created from the mast when there is a higher level of vorticity around the tips is of interest. Once again it is of great importance to remember that these results are not fully verified. But apart from the coarser mesh, there is nothing intending that these results are untrustworthy. These results would imply that the theory as well as the statement from Seldén are verified. That mast configuration (*a*) is indeed creating a larger noise than configuration (*b*). This can be seen if comparing Figure 4.7 and Figure 4.2. Presuming that this is correct it is of interest to look at Figure 4.6b and compare that to Figure 4.8a. It seems that in both cases the noise is generated by the vorticity created by the tips. It is then interesting to note that configuration (*a*) seems to generate more noise. Hence one could state that the design of mast configuration (*b*) helps to reduce the noise level.

From Section 2.1 it is know that sharp edges in general generate noise. This is due to the sudden blend of fluids at different pressure levels. If the Figures 4.6b and 4.8a are compared it is possible to see that there is vorticity around the tips in both cases. Note that the tips that are referred to in configuration (*b*) are the two enclosing the smaller hole for an extra sail. By comparing the sound level of these two cases, it can be seen that configuration (*a*) generates a higher noise. The main difference in the tip geometry is that in configuration (*a*) the distance between the tips is much larger than in configuration (*b*). From this one could claim that the amount of space after the edge would effect the capacity of noise that can be created.

Another interesting aspect to investigate is to regard the area inside the mast, where the two tips create an opening, as a resonance box. In music instruments, such as guitars, the strings create the vibration and with the help of the resonance box the tune is created. The empty space within the mast could possibly work as a resonance box. This would imply that it would be of interest to have as little empty space as possible within the mast in order to reduce the creation of noise. An example of noise that is created in a similar fashion is when you blow into a bottle. The more liquid that the bottle contains, the higher frequency the noise has. This is an effect of the amount of open space in the bottle. A full bottle barely produces any noise. This would therefore imply that it is of interest to make a sail, which when it is folded inside the mast, will fill out the entire cavity all through the mast.

Since numerical methods have been used in this project there is always a chance that there are some errors in the simulation set up. Especially so since the time frame was short in regards to the prior knowledge within aero-acoustics of the group. Unsteady 3D computations are demanding and require large resources, therefore the computations were time consuming. It would for instance have been desirable to use a larger domain than the one used in these simulations. Especially in the span-wise direction, where the domain had to be limited in order to attain a number of cells

that was low enough. The mesh itself may have been too coarse to fully resolve the correct aero-acoustic features. As a part of the simulations there was an aim to conduct an extensive mesh dependency study. This was partly abandoned due to difficulties in generating a mesh with sufficiently low number of cells. Thus the mesh generation process became very time consuming and valuable time was taken away from the simulations and post processing. In the start-up of the simulations large convergence problems occurred. This was mainly due to difficulties when setting up the physics for capturing the acoustics. Various boundary conditions and properties were therefore tested in order to acquire a converged solution. It should be emphasized that none of the group members had any previous experience in the aero-acoustic field.

5

Conclusion

The project goal was to explain the effects of the tip geometry in a mast regarding noise generation. It was concluded that the two mast geometries indeed do generate noise. However, from the case examined it cannot be verified that any of the two configurations creates a tonal noise. The results show that the vortex shedding was mainly caused by the bluff mast body itself and not the tips. Aero-acoustic theory suggests that the whistling should occur due to vortex shedding caused by sharp edges. Since the vorticity is low in the tips-region, no major whistling should be generated. It is the believe of the authors that other yaw angles might generate a whistling noise caused by the tips. But as for as now, one could not determine the root cause of the whistling noise.

During the project the experienced tonal noise could not be reproduced. No recommendations can therefore be made with certainty to Seldén Mast based on the results. However some interesting aspects regarding the flow around the mast have been identified and analyzed.

From this study alone, it cannot be concluded that mast (*a*) in general generates a higher tonal noise than mast (*b*). In order to fully understand the noise generation features it is thus recommended to conduct a more comprehensive investigation. A profound study should include several yaw angles and varying free stream velocities. A more extensive mesh dependency study would also be of interest. This is to ensure that the results are reliable enough.

Bibliography

- [1] Junker Miranda, U. (2009) *Bonniers Uppslagsbok*. ©Bonnier Fakta AB.
- [2] Goldsmith, . (2012). *DISCORD: The story of noise* Oxford University Press. ©Mike Goldsmith 2012.
- [3] Albrecht Wagner, C. Hütti, T. Sagaut, P (2007). *Large Eddy Simulation for Acoustics*. ©Cambridge University Press 2007.
- [4] Anselmet, P. Mattei, P.O. (2016). *Acoustics, Aeroacoustics and vibrations* ©ISTE Ltd 2016.
- [5] D. Olivari. (2012), *Von Kármán vortex shedding*, Retrieved from <https://www.encyclopediaofmath.org>
- [6] Powell A., *Why Do Vortices Generate Sound?*, ASME. J. Mech. Des. 1995;117(B):252-260. doi:10.1115/1.2836464.
- [7] Lars Davidson, (2017) *Fluid mechanics, turbulent flow and turbulence modeling*. Unpublished.
- [8] Lighthill, M. J. (1952). *On sound generated aerodynamically. I. general theory*. Proceedings of the Royal Society of London. Series A, Mathematical and Physical Sciences, 211(1107), 564-587.
- [9] Kaltenbacher, M., Escobar, M., Becker, S., and Ali, I. (2010;2009;). *Numerical simulation of flow-induced noise using LES/SAS and Lighthill's acoustic analogy*. International Journal for Numerical Methods in Fluids, 63(9), 1103-1122. doi:10.1002/fld.2123
- [10] Axel Kierkegaard (2016). *Best Practices for Direct Noise Calculations*.
- [11] Hua-Dong Yao Lars Davidson Lars-Erik Eriksson Shia-Hui Peng Olof Grundestam Peter E. Eliasson (2014), *Surface integral analogy approaches for predicting noise from 3D high-lift low-noise wings*, pp. 326-338.
- [12] F.J. McQuillan, J.R. Culham and M.M. Yovanovich (1984). *PROPERTIES OF DRY AIR AT ONE ATMOSPHERE*. Microelectronics Heat Transfer Lab University of Waterloo Waterloo, Ontario
- [13] Dong, Y., Yan, Y. & Liu, C. (2016), *New visualization method for vortex structure in turbulence by lambda2 and vortex filaments*, APPLIED MATHEMATICAL MODELLING, vol. 40, no. 1, pp. 500-509.
- [14] J. Jeong, F. Hussain (1995), *On the identification of a vortex*, J. Fluid Mech. 285 69–94.

